Marine and Petroleum Geology 145 (2022) 105921

Contents lists available at ScienceDirect

Marine and Petroleum Geology

journal homepage: www.elsevier.com/locate/marpetgeo

Characterization and classification of the microporosity in the unconventional carbonate reservoirs: A case study from Hanifa Formation, Jafurah Basin, Saudi Arabia

Mohamed O. Abouelresh [a,**], Mohamed Mahmoud [b], Ahmed E. Radwan [c,*], Thomas J.H. Dodd [d], Lingyun Kong [e,f], Hatem F. Hassan [g]

[a] Center for Environment and Marine Studies, RI, KFUPM, Saudi Arabia
[b] Petroleum Engineering Department, CPG, KFUPM, Saudi Arabia
[c] Faculty of Geography and Geology, Institute of Geological Sciences, Jagiellonian University, Gronostajowa 3a, 30-387, Kraków, Poland
[d] British Geological Survey, Lyell Center, Research Avenue South, Edinburgh, EH216ER, UK
[e] Energy & Environmental Research Center, University of North Dakota, Grand Forks, ND, USA
[f] Department of Petroleum Engineering, School of Earth Resources, China University of Geosciences, Wuhan, China
[g] Geology Department, Port Said University, Egypt

ARTICLE INFO

Keywords:
Microporosity
Organic-rich carbonate rocks
Unconventional resource
Solid bitumen
Coccolith tests
Hanifa formation

ABSTRACT

Formation porosity is a key factor that exerts substantial control upon reserve estimates, and ultimately may affect the development viability of unconventional resources. Microporosity studies have largely focused on siliciclastic mudstones, with limited examples that assess porosity type and distribution in organic-rich calcareous mudstone successions. In this work, a comprehensive porosity characterization study was performed on the organic-rich carbonate-dominated Hanifa Formation of the Jafurah Basin, which is the largest unconventional basin in Saudi Arabia. An extensive experimental program, involving petrographical description, SEM analysis, mineralogical analysis using XRD and QEMSCAN, and geochemistry analysis was employed in order to characterize the samples and analyze the geological origins of the microporosity. The main constituent minerals in this study are calcite (87 wt%) and anhydrite (9 wt%), as well as <1 wt% quartz, illite, pyrite, and dolomite. Total organic carbon reaches up to 5.46 wt %, yielding 5.09 mg HC/g rock (S2), while the free hydrocarbon content (S1) is 5.36 mg/g rock. Type II kerogens characterize the rock samples, and the thermal maturity index is 1.28. The microporosity in Hanifa Formation can be classified into three groups, including framework, solid bitumen, and intraparticle pores. Framework porosity is observed as the main type of microporosity, with solid bitumen representing a subordinate component of the overall porosity. Sheltered pores are also encountered associated with coccoliths tests deposited within the pelagic sediments. Higher degrees of thermal maturity of these sedimentary rocks increase the storage space for the generated hydrocarbon hosted in the solid bitumen. This study introduces an under-explored category of unconventional resources, nominally those that have a carbonate content >85%. Fundamentally, the findings of this study demonstrate that the Hanifa Formation in the Jafurah Basin has the potential for gas exploration and recovery.

1. Introduction

Due to the depletion of conventional oil and gas reservoir resources, unconventional reservoirs are becoming increasingly important in the field of hydrocarbon exploration and development (Radwan et al., 2022; Sohail et al., 2022). Unconventional reservoir characterization is considered as one of the major aspects in development of oil and gas in tight reservoirs (e.g., shale, tight carbonate rocks, tight sandstones, and coals). The pore structure or network in unconventional reservoirs is a fundamental component of understanding the capacity and potential of unconventional resources across different lithologies (Liu et al., 2017; Yan et al., 2017; Gao et al., 2020; Elsayed, 2022; Boutaleb et al., 2022)

* Corresponding author.
** Corresponding author.
E-mail addresses: abouelresh@kfupm.edu.sa (M.O. Abouelresh), radwanae@yahoo.com, ahmed.radwan@uj.edu.pl (A.E. Radwan).

https://doi.org/10.1016/j.marpetgeo.2022.105921
Received 16 April 2022; Received in revised form 31 August 2022; Accepted 13 September 2022
Available online 17 September 2022

and has attracted many researchers worldwide (Mehmani and Prodanović, 2014; Mayo et al., 2015; Ge et al., 2016; Ma et al., 2017; Sanaei et al., 2019; Zhang et al., 2022).

Three Late Jurassic formations (Tuwaiq Mountain, Hanifa and Jubaila) have been long recognized as the main source rocks for the supergiant Ghawar Oilfield (Cole et al., 1994). Recent analysis of source rocks within these formations has raised the possibility for a new frontier of unconventional shale gas exploration and development, particularly from the Tuwaiq Mountain and Hanifa formations in the Jafurah Basin (Fig. 1A and B), which is the most significant and recent exploration and production area in the Eastern Saudi Arabia (Hakami et al., 2016; Eltom et al., 2021; Weijermars et al., 2021). This study focuses on the Hanifa Formation, where previous research has highlighted the characterization of the depositional environments (e.g., Arkell et al., 1952; Ginsburg, 1956; Powers et al., 1966; Powers, 1968; Gischler et al., 2013; Al Ibrahim et al., 2017), diagenetic processes (e.g., Okla, 1983, 1986; Moshrif, 1984; Syahputra et al., 2022), and paleontology (Hughes, 2004, 2009; Hughes et al., 2008; and El-Sorogy and Al-Kahtany, 2015; Elzain et al., 2020). Porosity characterization is a key factor in unconventional tight play exploration within organic-rich rocks as the pore spaces are the location of hydrocarbon generation and storage. Unconventional oil and gas are stored in both inter-granular and intra-granular porosity, natural fractures, as well as being adsorbed and dissolved in kerogen and grain matrix surfaces (Curtis, 2002). Fundamentally, the microstructure of unconventional reservoirs controls the gas storage potential and flow properties through the porous network (Curtis et al., 2012; Liu and Ostadhassan, 2017).

Detailed petrographical analysis is an effective tool in the comparison of tight gas/oil formations across the world, with micro-porosity studies largely focused on the silica and clay-rich shale plays, including the Barnett Shale of the Fort Worth Basin (Loucks et al., 2009), the Woodford Shale of the Arkoma Basin (Slatt and O'Brien, 2011), and the Marcellus, Mahantango and Utica shales of the Appalachian Basin (Slatt and O'Brien, 2011; Song and Carr, 2020). These shale plays are considered as key case examples for all worldwide potential shale gas and other tight-reservoir resources (e.g., Davies et al., 1991; Dorsch, 1995; Dewhurst et al., 1999; Reed and Loucks, 2007; Ruppel and Loucks, 2008; Loucks et al., 2009; Nelson, 2009; Slatt and O'Brien, 2011). In-comparison, there are only a handful of studies that investigate the pore architecture in organic-rich carbonate and calcareous mudstones, such as those on the Eagle Ford and Niobrara formations (e.g., Loucks et al., 2012; Loucks and Rowe, 2014; Michaels and Budd, 2014).

Unconventional reservoirs, and in-particular those parts comprising mudstones, show strong textural and mineralogical heterogeneity at a range of different scales. Thus, a multi-scale characterization approach (e.g., like in Abouelresh, 2015; Yu et al., 2019; Arif et al., 2021) provides a representative and uniquely informative perspective of sample properties. Whilst analytical experimental methods for studying the pore morphology are available such as: Mercury Injection Porosimetry (MIP; Josh et al., 2012), Nuclear Magnetic Resonance (NMR; Sigal and Odusina, 2011), and Gas Adsorption (Huang et al., 2018), conventional imaging methods that directly observe the pore structures (such as Scanning Electron Microscope (SEM)-based petrography) retain considerable value for pore type and morphology identification, and characterization in unconventional plays (O'Brien et al., 2016). SEM analysis provides integrative information on the pore size, distribution, and connectivity at the micro to nano scale (e.g., Loucks et al., 2009; Curtis et al., 2012; Loucks et al., 2012; Milliken et al., 2013, 2014).

The main objective of this work is to provide a descriptive petrological characterization of the microporosity architecture in the organic-rich Hanifa Formation from Jafurah Basin, Saudi Arabia. This study describes and interprets the results of an extensive experimental program, involving petrographical description, SEM analysis, XRD analysis, QEMSCAN analysis, and geochemistry. It reveals the main constituent mineral types, free hydrocarbon content (S1), total organic carbon fraction (S2), kerogen type, and the thermal maturity index. Microporosity in the Hanifa Formation is classified into different groups to better evaluate the pore origins and associated surrounding mineralogy.

Through this analysis, this study answers the following key questions:

i. How was the microporosity developed and preserved in Hanifa Formation?
ii. How did the primary microporosity evolve with changes in thermal maturity?
iii. To what extent is there unconventional hydrocarbon potential in the Hanifa Formation?

The results of this study improve the overall geological understanding of the Hanifa Formation and provide important insights into the petrographical and microporosity characteristics of carbonate mudstone facies within the formation. Through this, the study provides a key case example for the microporosity character and resource potential within carbonate mudstone shale plays in-general.

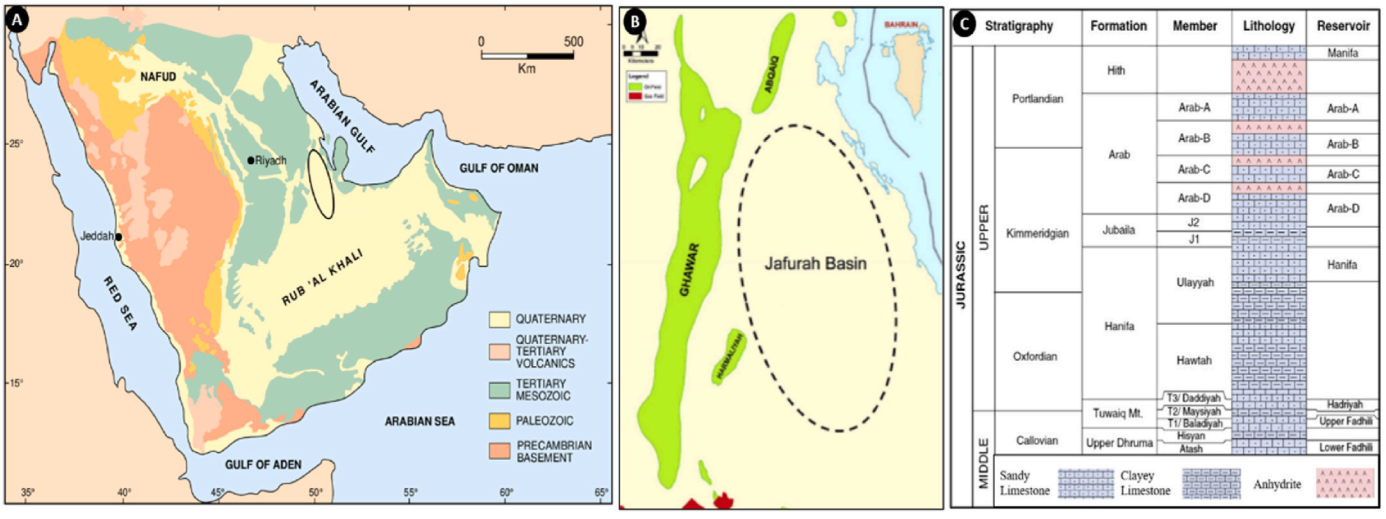

Fig. 1. (A) Generalized geological map of the Arabian Peninsula. (B) Regional-scale map, showing the Jafurah Basin located to the east of Ghawar Oil Field (modified after Hakami et al., 2016). (C) Generalized stratigraphy of the Middle to Upper Jurassic in the study area (modified after Sharland et al., 2001).

2. Geological setting

The Jafurah Basin is located within the central Arabian Intra-shelf basin in the eastern part of Saudi Arabia and is dominant by Jurassic sediments of varying depositional settings (Fig. 1A and B; Hakami et al., 2016). The rise and fall of eustatically-controlled relative sea level during the Jurassic resulted in the deposition and preservation of varied lithologies (Fig. 1C; Al-Husseini, 1997). As part of the Jurassic succession, the Oxfordian-aged Hanifa Formation mainly consists of marine carbonates deposited in the Arabian intrashelf during the marine transgression on the south-western side of the Neo-Tethys Ocean (Al-Husseini, 1997; Sharland et al., 2001). The Jurassic carbonate succession in Eastern Saudi Arabia was deposited on a platform, developed during a major transgression on the western margin of the Neo-Tethys Ocean (Murris, 1980; Al-Husseini, 1997; Hughes et al., 2008; Hakami et al., 2016). Stratigraphically, the Upper Jurassic sediments are divided into four formations, including (from base to top): the Hanifa, Jubaila, Arab and Hith formations (Fig. 1C). The Hanifa Formation overlies the Middle to Upper Jurassic Tuwaiq Mountain Formation.

The Hanifa Formation was deposited in a restricted marine environment, within an intra-shelf basin (Sharland et al., 2001). Typical lithofacies of the Hanifa Formation include 'laminated dark and light mudstones', 'brown bioturbated pack to wackestone', and 'palmate anhydrite' (Al-Ibrahim et al., 2017). The laminated dark and light mudstones are composed of darker intervals that have more mud and organic matter, and lighter intervals composed of sparite. The brown bioturbated packstones to wackestones contain grey to brown grains and are characterized by moderate to low bioturbation. The 'palmate anhydrite' is located at the top of the formation, where palmate structures exist within white to light grey anhydrite (Al-Ibrahim et al., 2017). This vertical lithological variation within the Hanifa Formation is thought to be largely controlled by relative sea level fluctuations (Hakami et al., 2016). The thickness of the Hanifa Formation in the Jafurah sub-basin ranges between 15 and 61 m (as reported by Hakami and İnan, 2016). The total organic carbon (TOC) of the Hanifa Formation reaches up to 14.3% (Cantrell et al., 2014).

3. Data and methodlogy

This study uses a combination of petrographical and geochemical analysis to better-understand the sedimentary deposits of the Hanifa Formation. Samples were analyzed using optical microscopy and scanning electron microscope (SEM) techniques, which were combined with X-ray diffraction (XRD) analysis, and organic geochemistry. The studied samples were further split and pulverized for petrographical analysis, rock-eval pyrolysis, quantitative evaluation of minerals by SEM (using QEMSCAN), backscattered electron microscope analysis (BSE), and additional SEM analysis.

3.1. Petrographical analysis

The core was sub-sampled into aliquots of millimeter-size fragments from 5 cm (1.9685-in.), which were collected from a depth interval between 1,2871 and 13,221 ft. Twenty representative rock samples were collected from Hanifa Formation for detailed petrographical modal analysis. Twenty thin sections were made to study the lithofacies characteristics, and to identify the rock components under polarizing microscope. The samples were treated with hydrochloric acid to remove carbonate minerals.

Descriptions of lithology, color, composition, and sedimentary structures were made. This paper applies the Dunham carbonate classification scheme (Dunham, 1962), in which carbonate sediments that are mud-supported and contain <10% grains are named mudstones, whereas those sedimentary rock types with >10% grains are classified as wackestone. Thin sections were observed using a polarizing Zeiss microscope ('Axio Scope A1').

Mineralogy and petrology were analyzed, including the quantitative analyses by XRD and qualitative observations of core and thin sections. The XRD analysis was performed using an 'XPert-Multipurpose Diffractometer' (Philips Corporation), comprising a copper butt, kV pipe pressure, a conduit flow of 40 mA, and a scanning speed of $(2\theta) = 2^{\circ}/$ min. As guided from preliminary optical microscope analysis of the studied facies, 12 representative thin sections were selected for mapping and mineralogical composition quantification using QEMSCAN® (Pirrie et al., 2004). Digital image analysis was applied in this work to quantitatively measure (using the 'Huang threshold'; Huang and Wang, 1995) the pore size, distribution, and pore characteristics (Huang and Wang, 1995; Camp, 2013; Pommer and Milliken, 2015). The thin sections were coated with carbon using a 'Q150T Quorum EMS 150R ES' and loaded into the 'QEMSCAN' instrument for analysis. This instrument is an automated system composed of a 'Quanta 650 FEG' SEM (made by 'Thermo Fisher Scientific'), two Energy Dispersive X-ray (EDX) spectroscopy detectors (made by 'XFlash' and 'Bruker Inc.'), and an extensive mineral database. This advanced petrographical technique has been used previously to analyze unconventional reservoirs (e.g., Tang et al., 2016; Kane et al., 2017; Hussain et al., 2021). The operation was carried out using an X-Ray beam produced by an accelerating voltage of 15 kV, and a sample current of 10 nA (±0.05). The 'field-scan' mode was selected with a covered area of 1 cm^2 and a point spacing of 5 μm. The data was acquired by 'iMeasure' and processed by the 'iDiscover' software. Preprocessors, such as field stitches, granulators, and boundary phase processors were applied. QEMSCAN analysis was conducted at the 'Center for Integrative Petroleum Research', King Fahd University of Petroleum & Minerals, Dhahran, Saudi Arabia. The 'Image J software', which was used in this study, is an open-source program created for the processing of porous media images (Schneider et al., 2012). SEM images are processed by the threshold tool to separate the observed pores from the matrix, thereby facilitating the calculation of pore area.

To identify the size, morphology and type of the micro-porosity, the investigated samples were scanned at a high-resolution (100 μm) using the in-house 'JEOL JSM 5900' SEM, which was operated with an accelerating voltage between 25 and 30 kV. The SEM analysis was carried out on six representative samples to examine and characterize the variety of diagenetic textures, mineral alterations, particle morphologies, and pore geometries. The fractured rock chips were coated with 2–3 mm of gold to stimulate the emission of secondary electrons, and to avoid the surface electron charging of the rock sample. The samples were studied using back scattered electron (BSE), as well as secondary electron (SE) imaging modes.

3.2. Geochemical analysis

The TOC was measured using a source rock analyzer ('LECO CS-200'), with an accuracy of 0.5%. Rock-Eval pyrolysis was performed using a 'Rock-Eval 6' analyzer to determine the level of free hydrocarbons (S1, mg HC/g rock), hydrocarbon generation from kerogen (S2, mg HC/g rock), and temperature of maximum S2 yield (T_{max}). Based on the TOC, S2, and S3 content, the hydrogen index (HI = [S2]/TOC mg HC/g TOC) and the oxygen index (OI = S3/TOC mg HC/g TOC) were calculated to characterize the likely origin of observed organic matter (OM).

The T_{max} value is a standardized parameter, calculated from the temperature at which the S2 peak reaches its maximum. HI and T_{max} were plotted against each other to classify kerogen types. The HI vs. oxygen index (OI), and 'HI vs. T_{max}' plots were used for the unconventional resources assessment (Behar et al., 2001).

4. Results

4.1. Petrographical analysis and depositional setting

4.1.1. Description

Petrographical analysis of the studied samples showed that the

lithofacies are composed of thinly-bedded (1–2 cm), laminated, light to dark black carbonate mudstones and wackestones. The matrix consists of coccoliths, peloids, siliceous sponge spicules, and some scattered thin-shelled bivalves (Fig. 2A and B). Coccoliths are micro-scale (<10 μm) calcite plates produced by phytoplankton of the marine algal group (McClelland et al., 2017). Although a large proportion of coccoliths were encountered broken, some samples retained their original structure. No visible porosity was observed in the thin section petrography. However, backscattered electron microscope (BSE) analysis showed the interparticle porosity is mainly filled with bitumen (Fig. 2C). Well-developed micro crystals of anhydrite were observed in this lithofacies (Fig. 2A and B). The XRD analysis indicates that calcite in the most dominant mineral in these samples (up to 87 wt%), while anhydrite accounts for 9.1 wt% on average (Table 1). Other minerals include quartz, illite, pyrite, and dolomite, which collectively form low proportions (3.9 wt%) of the total volume of the rock (Fig. 3A).

Thin section and SEM investigations show the existence of framboidal pyrite, partial pore-filling micrite microcrystals, and well-developed dolomite rhombohedral crystals (Fig. 2). The mineral distribution map acquired by QEMSCAN analysis (Fig. 3B) illustrates the dominance of calcite (83%) and anhydrite (*c.* 9%), with minor occurrences (≤1%) of quartz, pyrite, and dolomite. The mineral composition is consistent with the results of the XRD analysis, which validates the accuracy of the petrological analysis. QEMSCAN-imaged porosity reaches up to 3% and is predominantly interparticle (Fig. 3B).

4.1.2. Interpretation

Based on the preserved laminations, organic richness, abundance of mud-grade material, and high planktonic content, the studied lithofacies is interpreted as representing a lower slope to basinal environmental setting. Evidence of active transport and deposition, such as the presence of starved ripples, erosional surfaces, and basal intraclast layers have also been reported (Al-Ibrahim et al., 2017). The occurrence of pyrite indicates a direct precipitation from oversaturated solution under redox condition during the deposition of Hanifa Formation (Taylor and Macquaker, 2000). However, although the middle to late Jurassic times was overall characterized by eustatic sea-level rise, some portions of Hanifa Formation reflect intervals of sea-level fall with basin restriction that resulted in deposition of anhydrite (Sarg, 1988). If the bulk of the deposition did indeed occur on a lower slope to basinal setting, the presence of anhydrite may indicate periods of extreme sea level change.

Table 1
XRD bulk mineralogy result of the studied sample.

Mineral Name	Bulk XRD %
Calcite	87
Anhydrite	9.1
Quartz	1.6
Pyrite	1.2
Dolomite	0.6
Illite	0.5

However, a low energy marginal marine setting presents an equally possible alternative interpretation of the depositional environment for the Hanifa Formation. These settings can accumulate deposits formed by coccolith tests and sponge spicules, particularly if these bioclasts were sorted along and across bar systems by longshore processes. A marginal marine setting also explains the presence of observed anhydrite and to some extent pyrite, which may have formed during periods of episodic drying and/or restricted waters, respectively. The deposition and precipitation of these minerals in marginal marine settings is often intrinsically related to changes in relative sea level through time.

4.2. Geochemistry

The bulk organic geochemical data, TOC content, and Rock–Eval results of the analyzed samples are provide in Table 2. These calcareous mudstone samples contain 5.46 wt % TOC, yield 5.09 (mg HC/g rock) (S2), and display a free hydrocarbon content (S1) of 5.36 (mg HC/g rock).

The kerogen type and petroleum potential of the investigated samples were evaluated using 'HI vs. OI' and 'HI vs. T_{max}' diagrams (after Espitalié et al., 1977; Fig. 4 A, B). From this analysis, the studied samples were found to be type II kerogens. Based on measured T_{max} values of 469 °C, the in-place hydrocarbons belong to the condensate to wet gas maturity window. The production index (PI) is often referred to as the maturity level of the organic content; the samples in this study have a PI of 0.51 referring to the early gas window, which provides evidence for the high potential of the Hanifa Formation to form at least condensate or

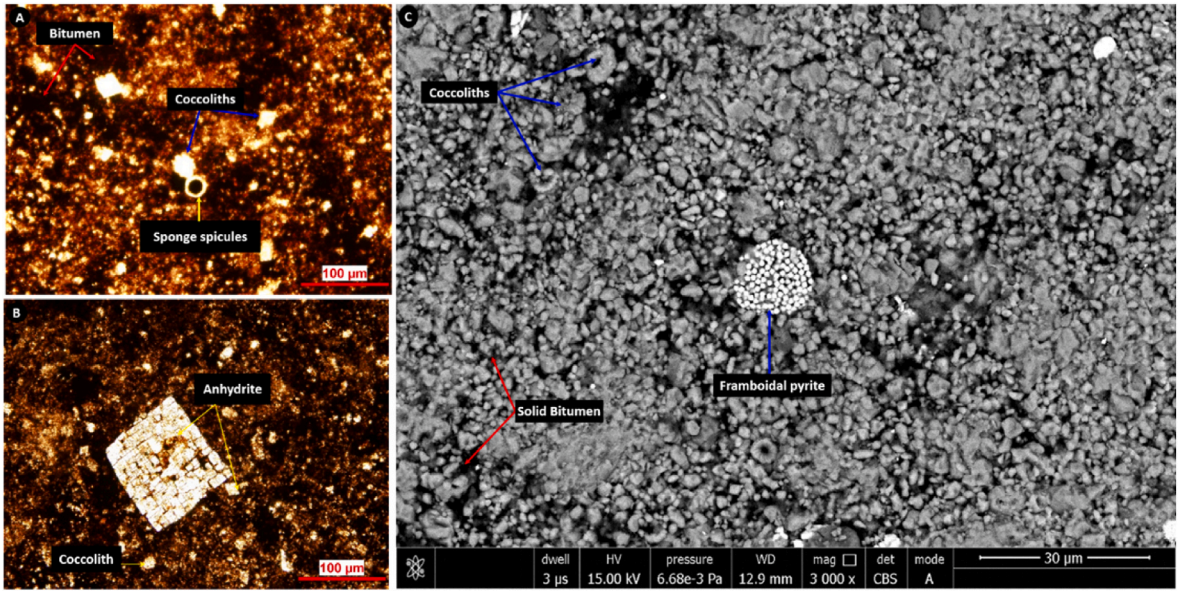

Fig. 2. Petrographical analysis of the organic-rich Hanifa Formation. (A) The groundmass is composed of micrite, with scattered coccoliths (shiny fragments), solid bitumen (black areas), and sponge spicules with bitumen-filled cores. (B) Thin section photomicrograph, showing the diagenetic crystallized anhydrite. (C) Backscattered image showing the main components of the studied rock; micrite microcrystals, coccolith tests, framboidal pyrite and solid bitumen that fill interparticle porosity.

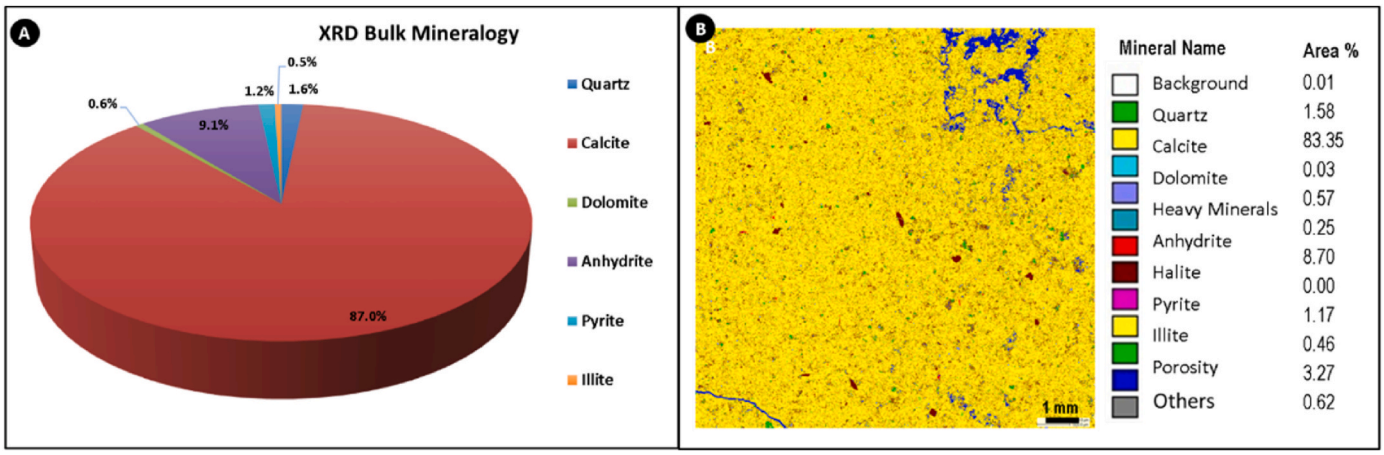

Fig. 3. XRD data and QEMSCAN analysis results. (A) Pie chart shows the XRD bulk mineralogy of the studied samples. (B) Mineral distribution map using QEMSCAN, showing the abundance of calcite (yellow color) relative to other components. (For interpretation of the references to color in this figure legend, the reader is referred to the Web version of this article.)

Table 2
Total organic carbon and programmed pyrolysis data.

TOC	S1	S2	S3	T_{max}	Calc.	HI	OI	PI
(wt%)	mg HC/g rock	mg HC/g rock	mg CO 2/g rock)	(°C)	%Ro	(mg HC/g TOC)	(mg CO 2/g TOC)	
5.46	5.36	5.09	0.42	469	1.28	93	7	0.51

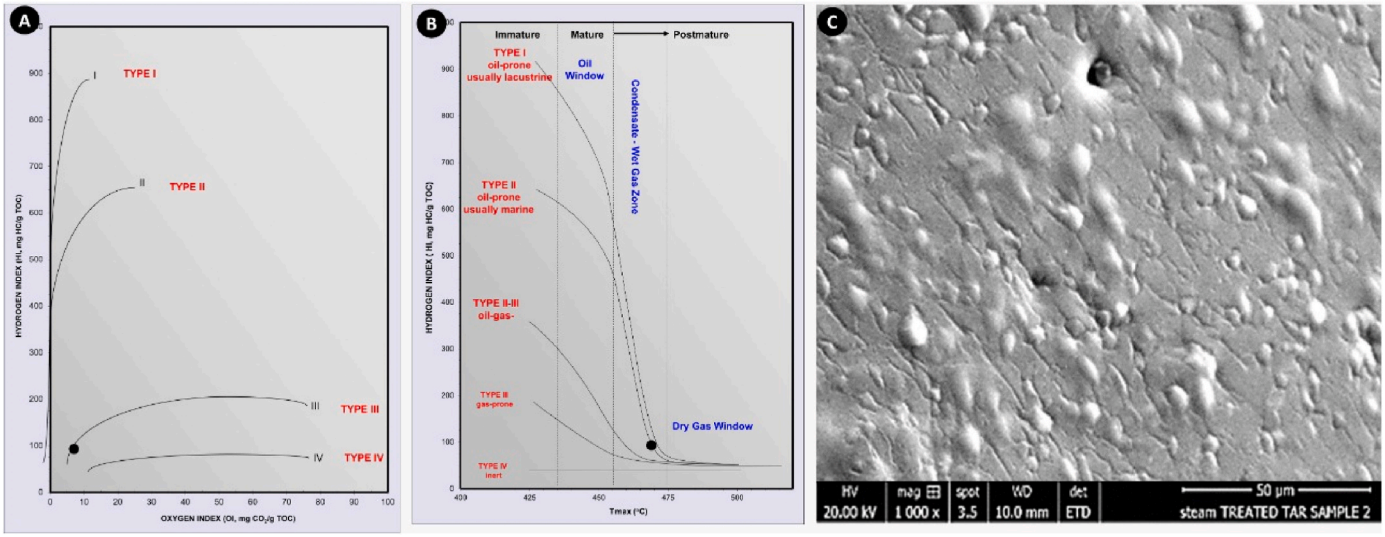

Fig. 4. Geochemical characterization of the studied samples. (A) Hydrogen index (HI) versus oxygen index (OI) plot (pseudo Van Krevelen), indicating Type II kerogens. B) HI versus T_{max} plot, showing the peak oil to wet gas windows. (C) Backscattered electron image of the downhole bitumen specimen with several micrite microcrystals.

gas-prone source rocks. The thermal maturity index R_o was calculated from T_{max} using the following empirical formula (*sensu* Jarvie et al., 2001):

$$\text{Calculated \% } VR_o = 0.0180 * T_{max}\ 7.16$$

Accordingly, the thermal maturity index of the studied samples is 1.28. A solid bitumen specimen was solid-like at room temperature, with a measured density of 1.03 g/cm^3, and an API gravity value of 6 (Fig. 4C). Asphaltene, resins, and aromatics represented 90% of the downhole bitumen sample.

4.3. Microporosity

Various types of pores in Hanifa Formation were identified using SEM analysis, including: (1) within framework components, herein referred to as 'framework pores', (2) organic-hosted pores, herein referred to as 'solid bitumen pores', and (3) inside grain pores, herein referred to as 'intragranular pores' (Fig. 5). Fracture porosity (or macro-porosity) is present within the Hanifa Formation samples, however it's contribution to the total porosity is considered either low or negligible. Based on the resolution of the obtained images, pores <1 µm in diameter are considered as 'nanopores', whilst those that measure >1 µm are categorized as 'micropores' (Loucks et al., 2012).

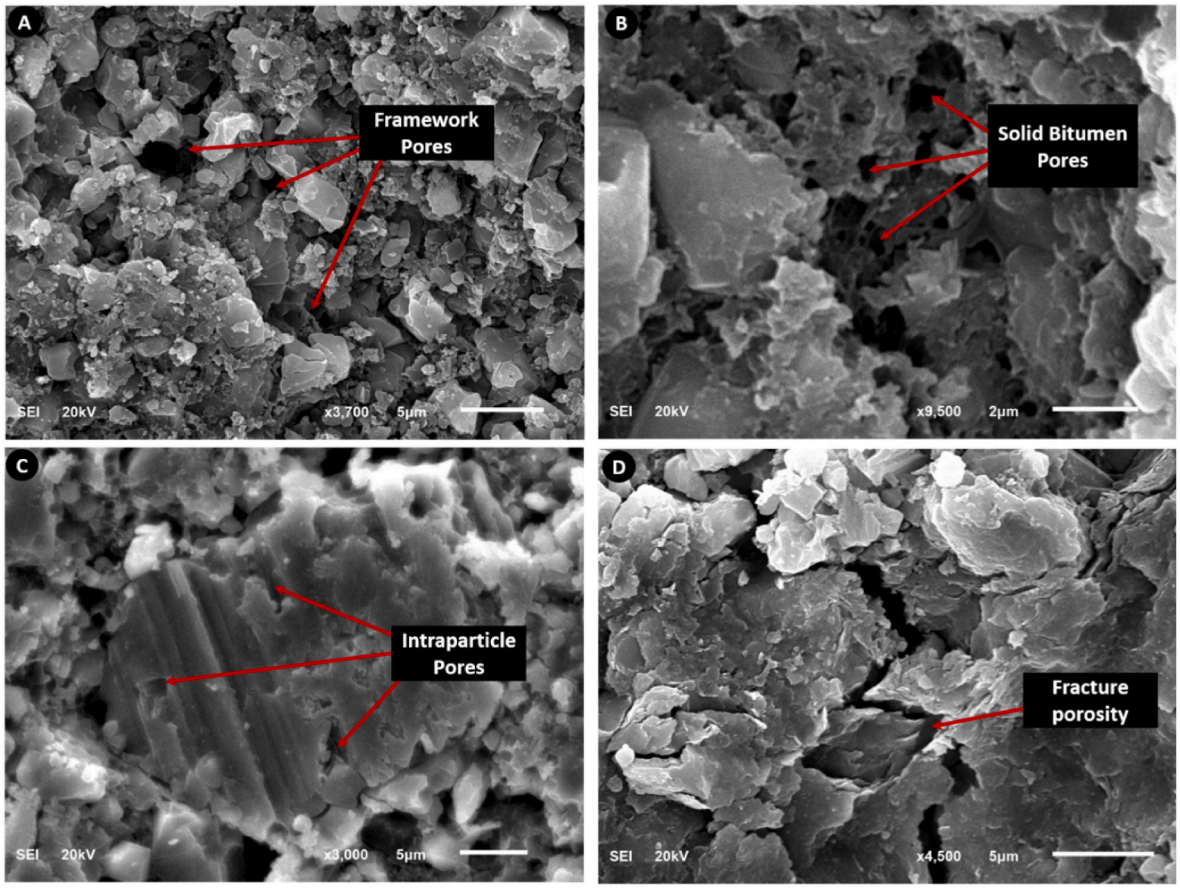

Fig. 5. SEM photomicrograph showing an overview of the main pore types. (A) Framework pores. (B) Solid bitumen pores. (C) Intraparticle pores. (D) Fracture porosity.

4.3.1. *Framework pores*

Framework pores include all types of primary pores that are identified by the authigenic components (skeletal and microfossil debris), and are formed during depositional processes (Schieber et al., 2016). This term is analogous to 'matrix pores' (*sensu* Rine et al., 2013), 'interparticle pores' as originally defined by Choquette and Pray (1970), and more-recently assigned to unconventional mudstones by Loucks et al. (2012). The framework pores, which include the pores between micrite microcrystals and inside the coccolith aggregates, are only occasionally observed in the studied samples (Fig. 5A).

Framework porosity associated with micrite reaches up to 5.5% on average, and when present it is largely filled with solid bitumen (Fig. 2C). In some cases, framework porosity developed due to the accumulation of coccoliths tests (Fig. 6D). The framework pores are commonly slot-like (tabular), ranging in size from 0.1 to 0.5 μm across, and up to 50–500 μm2 in area (Fig. 6 C, F). The intra-micrite-microcrystal pores range between ~0.1 and 0.5 μm in diameter and up to 2 μm in length. Fracture porosity was observed within the rock matrix, which is generally <5 μm in width (Fig. 6G–I).

4.3.2. *Solid bitumen pores*

Solid bitumen forms as the insoluble remains from organic matter after oil and gas generation and migration into, and through available porous and permeable material (Reed et al., 2012). It mainly fills the interparticle porosity and embayments within euhedral micrite microcrystals and pyrite framboids, which is in contrast with primary organic matter particles or kerogen that retain their original morphologies (Hunt, 1996; Bernard et al., 2012; Loucks and Reed, 2014; Cardott et al., 2015; Mastalerz et al., 2018).

The existence of solid bitumen in the samples was observed during the petrographical analysis (Fig. 3C). In the SEM images, the solid-bitumen-filled pore morphology is 'sponge-like', with pore radii as much as ~1.0 μm, forming round to oval irregular shapes, with relatively well-defined boundaries, which demonstrates a high level of connectivity (Fig. 7A and D). The solid-bitumen-filled pore areas range between 200 nm and 500 nm and the pore radii ranged between 0.2 and 0.3 μm (Fig. 7B, C, 7E and 7F). These quantitative data obtained from SEM analysis illustrates the difference between solid bitumen and framework porosity.

4.3.3. *Intraparticle pores*

Intraparticle pores form within a wide variety of particle types, including within the framework grains, in fossil tests, or within framboidal pyrite minerals. Typical intraparticle pores were observed within fully open and broken coccolith tests (Fig. 8A and B), as well as in core channels of sponge spicules (Fig. 8C). Partial dissolution of the coccolith tests likely resulted in the formation of ~2–10 μm wide intraparticle pores (Fig. 8D). Additionally, diagenetic cementation provides some intraparticle porosity between authigenic micrite crystals, especially those that are lined with organic material (Fig. 8E). Framboidal pyrite also exists in the studied samples, commonly co-existing with OM, and developing additional intraparticle porosity (Fig. 8F).

Sheltered porosity includes all spaces created due to the structure of the most abundant pelagic tests (in this case coccoliths; Harbaugh, 1967). Additionally, porosity is developed due to the random accumulation process and resultant poor-sorting of coccolith tests. In most cases, the sheltered porosity forms conical shapes (Fig. 6D), and therefore belongs to the standard intraparticle pore category (*sensu* Slatt et al., 2013). Complete coccoliths tests (Fig. 8A and B) show that bitumen filled these pore spaces likely early in the burial history, preserving the

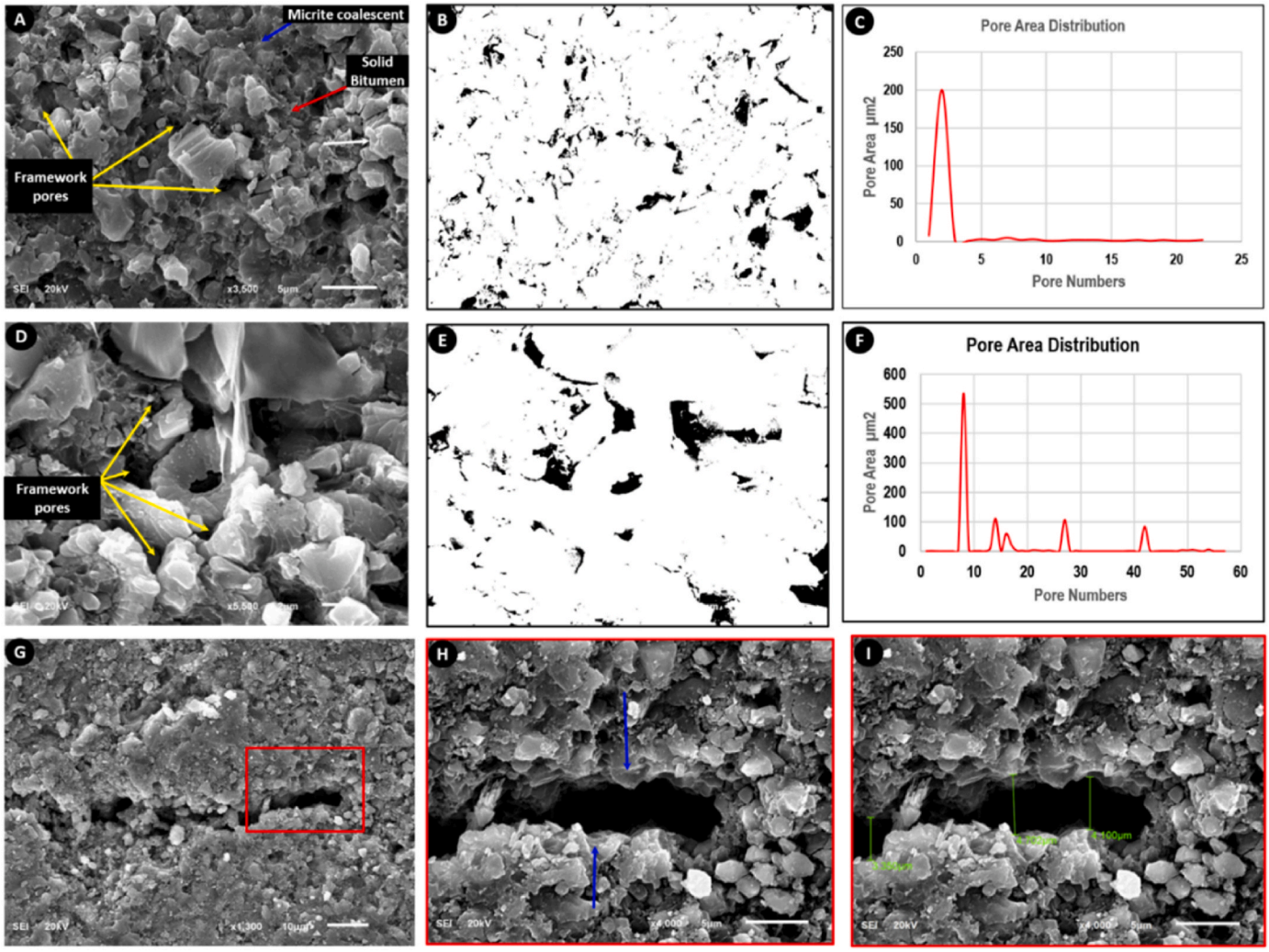

Fig. 6. SEM photomicrograph showing framework porosity. (A) Framework porosity (yellow arrow) between micrite coalescent (blue arrow) and a broken coccolith test (white arrow). Note solid bitumen filling porosity (red arrow). (B) Threshold adjusted image of part A, showing isolated pores in black, within the white framework. (C) Distribution histogram of pore spaces versus area in µm2. (D) Framework porosity (yellow arrows) formed through the accumulation of coccolith tests. (E) Threshold adjusted image of part D, showing the isolated pores in black and framework in white, with pore area distribution plotted in a histogram (F). (G) Microfracture in the studied samples enlarged in part (H), where diagenetic micro micrite crystals (blue arrow) developed on the fracture surface. (I) SEM image shows the width (~4 µm) of the same fracture. (For interpretation of the references to color in this figure legend, the reader is referred to the Web version of this article.)

original porosity (to some extent) before significant compaction occurred. It is also possible that sheltered porosity is reduced by diagenetic micrite cementation, however the dissolution of coccoliths plates through diagenesis also has the potential to positively-contribute to overall porosity.

5. Discussion

5.1. Microporosity characterization in carbonate versus clastic mudstones

Research into unconventional reservoirs, particularly their microscopic pore-space, represents a key part of the workflow for resource evaluation, exploration, and development of tight gas and oil resources (e.g., Chalmers et al., 2012; Jiao et al., 2014; Ma and Holditch, 2015; Ge et al., 2016; Rahner et al., 2018; Goral et al., 2019; (Radwan et al., 2021) Radwan et al., 2021). The pore system in tight reservoirs is influenced by the interaction of mineralogical composition, diagenesis, and organic matter maturation, which also controls the mechanical properties. Micro and nanopores form the key seepage channels during gas development and provide the gas accumulation space within tight unconventional reservoirs (Yang et al., 2019). The developed pores in unconventional reservoirs include organic-matter pores, diagenetic fractures, inter-crystal pores (authigenic or related to recrystallization) of matrix minerals, micro-fractures, and residual pores (Yang et al., 2019). The quartz, clay, and calcite content play a significant role in the pore system development in tight unconventional resources.

One of the main issues when examining carbonate reservoirs is the context of how they are being used; whether they are targeted as a conventional hydrocarbon reservoir or form a key stratigraphic unit in unconventional hydrocarbon exploration plays. The porosity in conventional carbonate reservoirs is mainly controlled by pre-existing porosity established by original depositional environments, or later by early diagenesis (Choquette and Pray, 1970). By contrast, in unconventional organic-rich carbonate reservoirs, preserved organic matter is the major contributor to pore network development (Lu et al., 2015; Ko et al., 2017). Ultimately, their intended use dictates how the storage space of the carbonate reservoirs is evaluated. This is of particular importance when characterizing and discussing the reservoir potential of the Hanifa Formation, which contains >85% calcite.

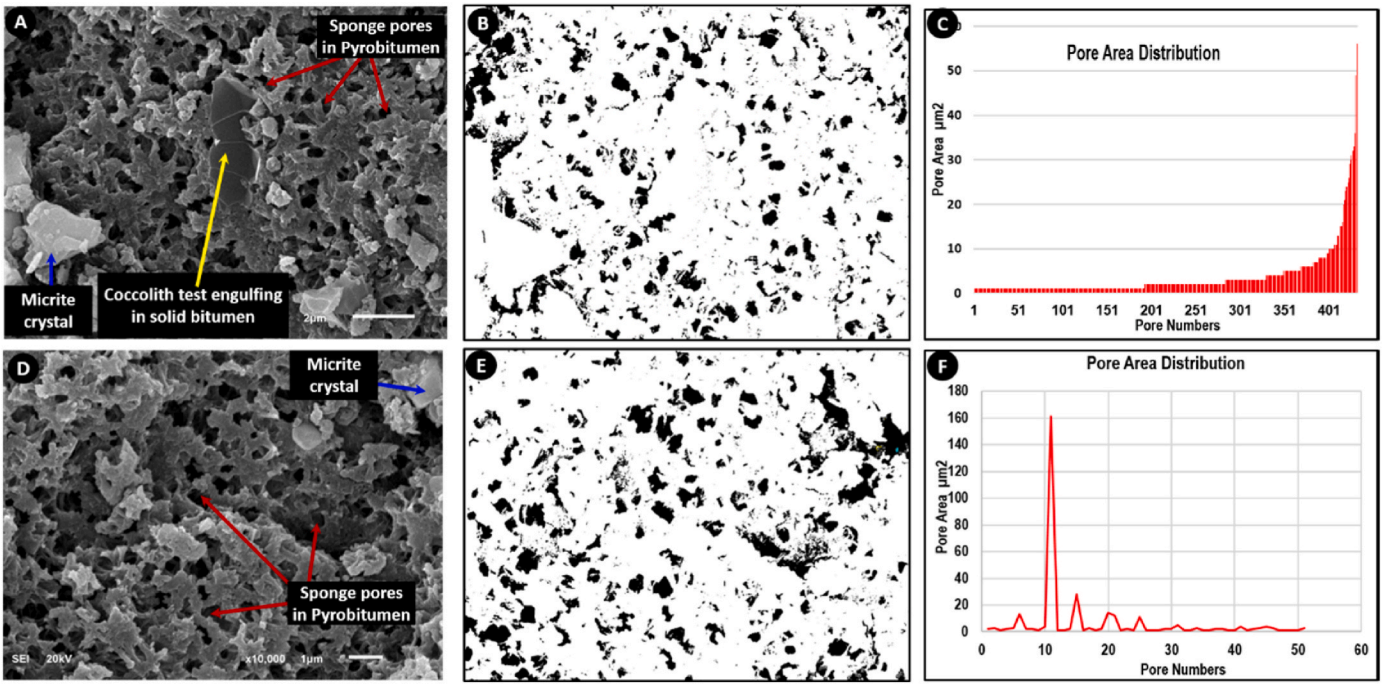

Fig. 7. SEM photomicrographs showing solid bitumen porosity. (A) An overview of the solid bitumen area, with extensive sponge-like pores. (B) Threshold adjusted image of part A, showing the isolated porosity in black and non-porous bitumen in white. (C) Distribution chart of pores versus pore area in µm^2. (D) Sponge-like pores reflect high connectivity in solid bitumen. (E) Threshold adjusted image of part D, showing the isolated porosity in black and non-porous bitumen in white. (F) Distribution chart of pore numbers versus pore area, with the majority of pores being <20 µm^2 in area.

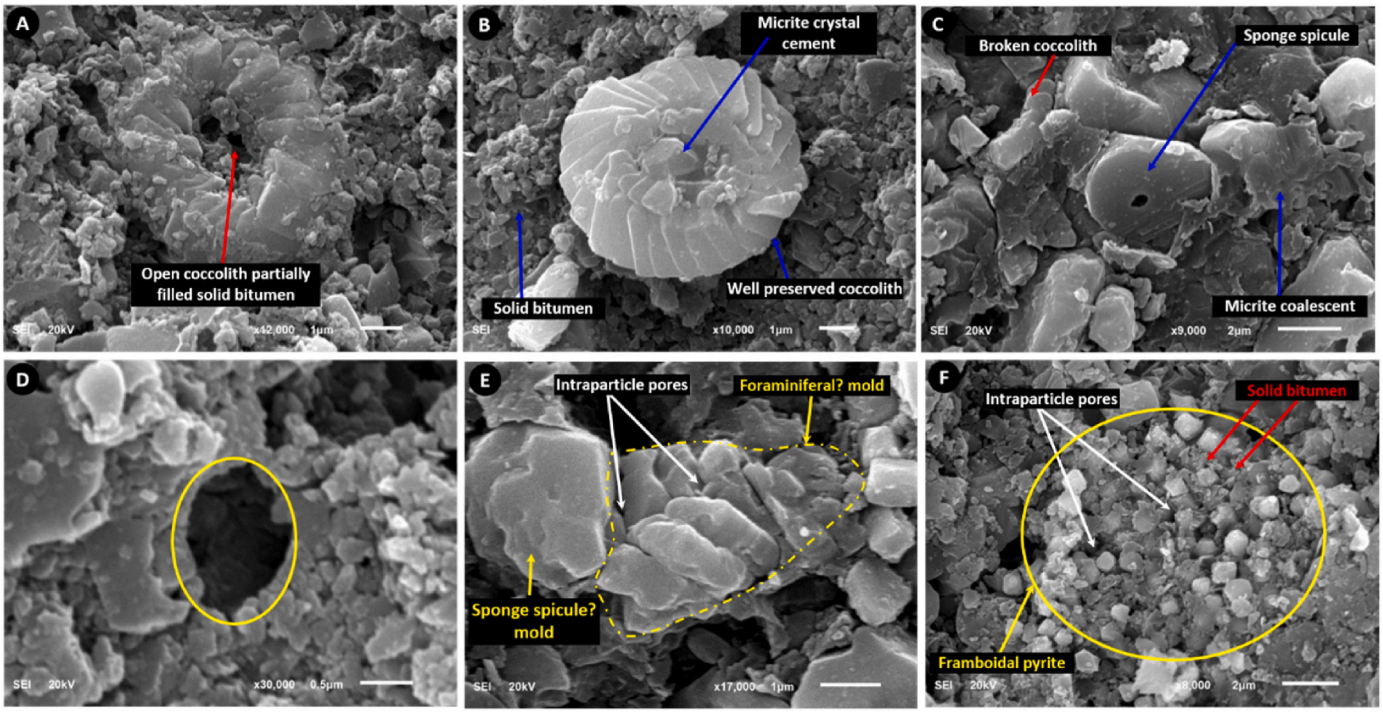

Fig. 8. SEM photomicrograph of intraparticle porosity and diagenesis effect. (A) intraparticle porosity in a coccolith test with an open core, which has been partially cemented. (B) Diagenetic micrite crystallization blocks the core of coccolith test. (C) A sponge spicule with an open core filled with solid bitumen. (D) Micro-vuggy pore resulting from selective dissolution of coccolith tests. (E) Diagenetic micrite recrystallized inside framework component (possibly a foraminifera and sponge spicule) forming molds and associated secondary intraparticle porosity (red arrows). (F) Framboidal pyrite (yellow circle) developed within the framework components holding some intraparticle pores (yellow arrows). (For interpretation of the references to color in this figure legend, the reader is referred to the Web version of this article.)

5.2. Pore type distribution and controls in the Hanifa Formation

The pore size forms one of the key descriptors when characterizing pore architecture (Beth and Grammer, 2016). Standard classification of pore types in carbonate mudstones has been proposed in seminal works based on the pore size, spatial relationship of pores with respect to the hosted textures, pore geometry, and diagenesis (Archie, 1952; Dunham, 1962; Folk, 1962; Choquette and Pray, 1970; Lucia, 1983, 1995; Rouquerol et al., 1994; Loucks et al., 2012; Fournier et al., 2018; Fang et al., 2021). In this study, 'carbonate mudstone' is used in relation to calcareous mudstone. However, it is important to highlight that no distinction between calcareous and siliciclastic mudstone is provided in the Dunham classification scheme, which is based on textural observations. Therefore, in-theory the method of describing the microporosity applies both to calcareous and siliciclastic mudstones. The use of these classification schemes relies upon the application of a range of techniques used to study porosity, which is somewhat limited by the resolution and quality of those datasets.

A key observation of this study is that pore types in Hanifa Formation vary between framework porosity that accounts for *c.* 25% of the measured pore areas, and intraparticle porosity that contributes *c.* 15%. The organic-hosted porosity forms a significant component of overall porosity within the Hanifa Formation, with up to 60% of the measured pore areas. The general absence of primary porosity is due to either the fine-grained nature of the studied lithologies (mudstones to wackestones), or to the widespread filling of solid bitumen. Sheltered pores are commonly associated with coccolith tests due to their morphological structure and random aggradational patterns from pelagic fall-out-type sedimentation (Figs. 6D and 9A). Due to the abundance of coccoliths in the Hanifa Formation (Hughes et al., 2008; El-Sorogy et al., 2018), shelter type often accounts for a considerable proportion of porosity in these reservoirs/target intervals.

In this study, the diagenetic micrite crystals showed a range of microtextures, ranging between rounded to sub-rounded, anhedral to subhedral crystals, with smooth faces and partially coalescent contacts (Fig. 9A). Recrystallization of sparite crystals on fracture boundaries (as shown in Fig. 6H and I) may negatively affect the permeability of the reservoir rock. The co-existence of framboidal pyrite and organic matter is very common in the organic-rich rocks (Fig. 9A). Moreover, as pyrite is a brittle mineral, it can act to increase the brittleness of organic-rich rock and hence increase the impact of hydraulic fractures for production purposes. This has the potential to promote hydrocarbon generation ability of the associated organic matter and consequently increases the number of organic-hosted pores (Ma et al., 2017).

Both intraparticle and interparticle organic micropores are the most essential parameter to evaluate the hydrocarbon potential of the Hanifa Formation, especially because both types strongly reflect the size, shape, and thermal maturation history of the organic content. Solid bitumen refers to the insoluble remains of kerogen after oil and gas generation (Hunt, 1996) and therefore is an indicator for past hydrocarbon generation and/or migration. The identification of solid bitumen in these samples was made, largely based on its irregular morphology and distribution, which is shaped by the intergranular primary porosity and is unlike the kerogen that has distinctive grain boundaries (Mastalerz

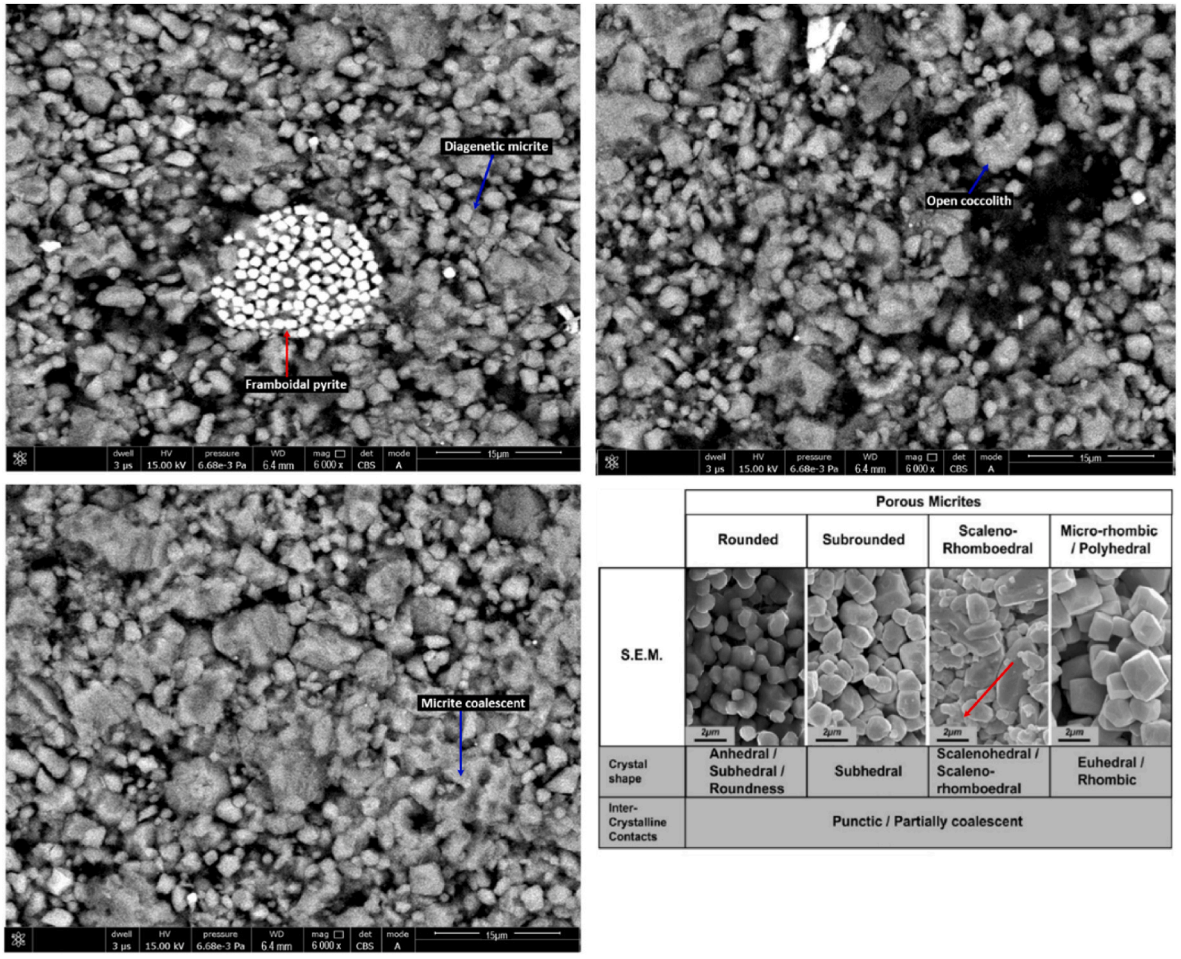

Fig. 9. BSE photomicrographs. (A) A BSE photomicrograph showing the digenetic framboidal pyrite and subhedral micrite crystals developed on the authigenic components. (B) BSE photomicrograph showing the framework porosity filled with solid bitumen. (C) BSE photomicrograph showing the micrite coalescent, as well as the subhedral crystals, reflecting the variation in diagenetic effects. (D) Classification scheme of micrite crystals (Deville De Periere et al., 2011).

et al., 2018). Also, the engulfing of solid bitumen to some authigenic components (coccoliths, sponge spicules and others) indicates the secondary migration of bitumen.

5.3. Unconventional hydrocarbon potential within the Hanifa Formation

The Hanifa Formation is considered as the main source rock for oil production in the supergiant Ghawar Field and is within both the oil and gas window. The existence of solid bitumen as the pore-filling material in the studied samples is therefore important to explore in the context of unconventional reservoir potential (Hakami and İnan, 2016). Solid bitumen is characterized by a distinctive pore shape, sponge-like morphologies (Loucks et al., 2012), and fenestra (Choquette and Pray, 1970). Image analysis shows that a single area of solid bitumen with a diameter of 1–5 μm could contain hundreds of sponge-like pores (Fig. 7D). Fenestra structures are commonly observed in many unconventional reservoirs and are typically formed due to the escape of both oil and gas after generation (Schieber, 2013). Sponge-like pores are an important component of the pore system in the Hanifa Formation and in other parts of the world have proved to contribute to the permeability in some shale gas plays (e.g., the Barnett Shale in the US (Jarvie et al., 2007). The simple association between more-numerable pores filled with bitumen and the associated increase in surface area for gas adsorption, will result in high gas in place estimates (GIP). This type of porosity presents an ideal mode for gas adsorption due to the high exposed surface areas of bitumen, and the equally high connectivity between micropores (Klaver et al., 2015).

Therefore, the findings of this study are important in terms of understanding type and distribution of pore systems in Hanifa Formation, which are the essential requirements for gas in place estimates, and ultimately evaluation of both conventional hydrocarbon plays and unconventional hydrocarbon reservoir potential. The results of this study also inform the hydraulic fracture propagation methodologies during future potential production.

6. Conclusion

The Hanifa Formation represents one of the most important unconventional targets within the Jafurah Basin, in the eastern province of Saudi Arabia. Microporosity and petrological analysis of the Hanifa Formation was conducted in this study, which found that the formation consists mainly of laminated organic-rich mudstones and wackestones, with TOC values up to 14.3%. The main minerals in the studies samples include calcite (87 wt%), anhydrite (9 wt%), as well as <1 wt% quartz, illite, pyrite, and dolomite. Through this analysis, three pore types have been identified in the Hanifa Formation, including framework pores, solid bitumen pores, and intraparticle pores. A significant proportion of porosity is observed associated with the organic content. Sheltered pores are commonly associated with coccolith tests, which is the dominant pelagic sediment in Hanifa Formation. Solid bitumen, characterized by sponge-like pore morphologies, formed due to escaping of both oil and gas after generation. Sponge-like pores are an important component of pore system in the Hanifa Formation. The classification and interpretation of the microporosity in this study provides important insights into the petrographical understanding of organic-rich calcareous mudstone, in general.

Credit author statement

Mohamed O. Abouelresh: Conceptualization, Methodology, Software, Investigation, Writing- Original draft preparation, Reviewing and Editing, Mohamed Mahmoud: Conceptualization, Methodology, Software, Investigation, Writing- Original draft preparation, Reviewing and Editing, Ahmed E. Radwan: Conceptualization, Methodology, Software, Investigation Writing- Original draft preparation, Reviewing and Editing, Thomas J.H. Dodd: Writing- Original draft preparation, Reviewing and Editing,Lingyun Kong: Writing- Original draft preparation,Reviewing and Editing,Hatem F. Hassan: Conceptualization, Methodology, Software, Investigation Writing- Original draft preparation, Reviewing and Editing.

Declaration of competing interest

The authors declare that they have no known competing financial interests or personal relationships that could have appeared to influence the work reported in this paper.

Data availability

Data will be made available on request.

Acknowledgments

The authors would like to acknowledge the support provided by the Deanship of Scientific Research (DSR) at King Fahd University of Petroleum & Minerals (KFUPM) for funding this work through project No. SB191041. The authors are grateful to Mr. Hatim Dafalla, Center for Engineering Research, and Mr. Abdullah Alqubalee, for their help in SEM and QEMSCAN analysis. Dr. Ahmed E. Radwan is thankful for the support provided by the Priority Research Area Anthropocene under the program “Excellence Initiative—Research University” at the Jagiellonian University in Kraków. This paper is published by permission of the Executive Director, British Geological Survey (UKRI).

References

Abouelresh, M., 2015. Quantitative and Qualitative Evaluation of Micro-porosity in Qusaiba Hot Shale, Saudi Arabia. Extended Abstract for paper presented at the Unconventional Resources Technology Conference, San Antonio, Texas. https://doi.org/10.15530/urtec-2015-2154081.

Al-Ibrahim, M.A., Sarg, J.F., Hurley, N., Cantrell, D.L., Humphrey, J.D., 2017. Depositional environments and sequence stratigraphy of carbonate mudrocks using conventional geologic observations, multiscale electrofacies visualization, and geochemical analysis: the case of the Tuwaiq Mountain and Hanifa Formations in a basinal setting, Saudi Arabia. AAPG (Am. Assoc. Pet. Geol.) Bull. 101 (5), 683–714.

Al-Husseini, M., 1997. Jurassic sequence stratigraphy of the western and southern Arabian Gulf. GeoArabia 2 (4), 361–382.

Archie, G.E., 1952. Classification of carbonate reservoir rocks and petrophysical considerations. AAPG (Am. Assoc. Pet. Geol.) Bull. 36, 278–298.

Arif, M., Mahmoud, M., Zhang, Y., Iglauer, S., 2021. X-ray tomography imaging of shale microstructures: a review in the context of multiscale correlative imaging. Int. J. Coal Geol. 233, 103641.

Arkell, W.J., Bramkamp, R.A., Steineke, M., 1952. Jurassic ammonites from Jebel Tuwaiq, central Arabia. Phil. Trans. Roy. Soc. Lond. B Biol. Sci. 241–313.

Behar, F., Beaumont, V., Penteado, H.D.B., 2001. Rock-Eval 6 technology: performances and developments. Oil Gas Sci. Technol. 56, 111–134.

Bernard, S., Wirth, R., Schreiber, A., Schulz, H.M., Horsfield, B., 2012. formation of nanoporous pyrobitumen residues during maturation of the Barnett shale (Forth Worth Basin). Int. J. Coal Geol. 103, 3–11.

Beth, V.B., Grammer, G.M., 2016. 2-D pore architecture characterization of a carbonate mudrock reservoir: insights from the mid- continent “Mississippi Lime”. In: Olson, T. (Ed.), Imaging Unconventional Reservoir Pore Systems: AAPG Memoir 112, pp. 185–232.

Boutaleb, K., Baouche, R., Sadaoui, M., Radwan, A.E., 2022. Sedimentological, petrophysical, and geochemical controls on deep marine unconventional tight limestone and dolostone reservoir: Insights from the Cenomanian/Turonian oceanic anoxic event 2 organic-rich sediments, Southeast Constantine Basin, Algeria. Sediment. Geol. 429, 106072 https://doi.org/10.1016/j.sedgeo.2021.106072.

Camp, W.K., 2013. Enhancing SEM grayscale images through pseudocolor conversion: examples from Eagle Ford, Haynesville, and marcellus shales. In: Unconventional Resources Technology Conference. Denver, Colorado, pp. 2300–2307.

Cantrell, D.L., Nicholson, P.G., Hughes, G.W., Miller, M.A., Bhullar, A.G., Abdelbagi, S.T., Norton, A.K., 2014. Tethyan petroleum systems of Saudi Arabia. In: Marlow, L., Kendall, C., Yose, L. (Eds.), Petroleum Systems of the Tethyan Region, vol. 106. AAPG Memoir, pp. 613–639.

Cardott, B.J., Landis, C.R., Curtis, M.E., 2015. Post-oil solid bitumen network in the Woodford Shale, USA – a potential primary migration pathway. Int. J. Coal Geol. 139, 106–113.

Chalmers, G.R., Bustin, R.M., Power, I.M., 2012. Characterization of gas shale pore systems by porosimetry, pycnometry, surface area, and field emission scanning electron microscopy/transmission electron microscopy image analyses: examples from the Barnett, Woodford, Haynesville, Marcellus, and Doig units. AAPG Bull. 96 (6), 1099–1119.

Choquette, P.W., Pray, L.C., 1970. Geologic nomenclature and classification of porosity in sedimentary carbonates. AAPG (Am. Assoc. Pet. Geol.) Bull. 54, 207–250.
Cole, G.A., Carrigan, W.J., Colling, E.L., Halpern, H.I., Al-Khadhrawi, M.R., Jones, P.J., 1994. The organic geochemistry of the Jurassic petroleum system in Eastern Saudi Arabia. Can. Soc. Petrol. Geol. Mem. 17, 413–438.
Curtis, J.B., 2002. Fractured shale-gas systems. AAPG Bull. 86 (11), 1921–1938.
Curtis, M.E., Sondergeld, C.H., Ambrose, R.J., Rai, C.S., 2012. Microstructural investigation of gas shales in two- and three-dimensions using nanometer-scale resolution imaging. AAPG (Am. Assoc. Pet. Geol.) Bull. 96, 665–677. https://doi.org/10.1306/08151110188.
Davies, D.K., Bryant, W.R., Vessell, R.K., Burkett, P.J., 1991. Porosities, permeabilities and microfabrics of Devonian shales. In: Bennett, R.H., Bryant, W.R., Hulbert, M.H. (Eds.), Microstructure of Fine-Grained Sediments: from Mud to Shale. Springer-Verlag, New York, pp. 109–119.
Deville De Periere, D., Durlet, C., Vennin, E., Lambert, L., Bourillot, R., Caline, B., Poli, E., 2011. Morphometry of micrite particles in Cretaceous microporous limestones of the middle east: influence on reservoir properties. J. Marine Petrol. Geol. 28, 1727–1750.
Dewhurst, D.N., Yang, Y., Aplin, A.C., 1999. Permeability and fluid flow in natural mudstones. In: Aplin, A.C., Fleet, A.J., Macquaker, J.H.S. (Eds.), Muds and Mudstones: Physical and Fluid Flow Properties, vol. 158. Geological Society of London: Special Publication, pp. 23–43.
Dorsch, J., 1995. Determination of Effective Porosity of Mud Rocks – A Feasibility Study. Oak Ridge National Laboratory, ORNL/GWPO-019, p. 60.
Dunham, R.J., 1962. Classification of Carbonate Rocks According to Depositional Texture: AAPG Memoir 1: Classification of Carbonate Rocks – A Symposium, p. 108.
Elsayed, M., et al., 2022. A review on the applications of nuclear magnetic resonance (NMR) in the oil and gas industry: laboratory and field-scale measurements. J. Pet. Explor. Prod. Technol. 12, 2747–2784. https://doi.org/10.1007/s13202-022-01476-3.
El-Sorogy, A.S., Al-Kahtany, K.M., 2015. Contribution to the Scleractinia corals of Hanifa formation, upper Jurassic, jabal al-abakkayn Central Saudi Arabia. Hist. Biol. 27 (1), 90–102.
El-Sorogy, A.S., Al-Kahtany, K.M., Almadani, S., Tawfik, M., 2018. Depositional architecture and sequence stratigraphy of the upper Jurassic Hanifa formation, central Saudi Arabia. J. Afr. Earth Sci. (139), 367–378.
Eltom, H.A., Alqubalee, A., Yassin, M.A., 2021. Potential overlooked bioturbated reservoir zones in the shallow marine strata of the Hanifa Formation in central Saudi Arabia. Mar. Petrol. Geol. 124, 104798.
Elzain, H.E., Abdullatif, O., Senapathi, V., Chung, S.Y., Sabarathinam, C., Sekar, S., 2020. Lithofacies modeling of Late Jurassic in upper Ulayyah reservoir unit at central Saudi Arabia with inference of reservoir characterization. J. Petrol. Sci. Eng. 185, 106664.
Espitalié, J., Madec, M., Tissot, B., Mennig, J.J., Leplat, P., 1977, May. Source rock characterization method for petroleum exploration. In: Offshore Technology Conference. OnePetro.
Fang, X., Feng, H., Wang, H., Wang, Y., 2021. Study on origin, classification, and identification of complex porous carbonate reservoir: a case study of the middle cretaceous Mishrif Formation in W Oil field. Carbonates Evaporites 36 (4), 1–17.
Folk, R.L., 1962. Spectral subdivision of limestone types. In: Ham, W.E. (Ed.), Classification of Carbonate Rocks – A Symposium: AAPG Memoir 1, pp. 62–84.
Fournier, F., Pellerin, M., Villeneuve, Q., Teillet, T., Hong, F., Poli, E., Hairabian, A., 2018. The equivalent pore aspect ratio as a tool for pore type prediction in carbonate reservoirs. AAPG (Am. Assoc. Pet. Geol.) Bull. 102 (7), 1343–1377.
Gao, Z., Fan, Y., Xuan, Q., Zheng, G., 2020. A review of shale pore structure evolution characteristics with increasing thermal maturities. Adv. Geo-Energy Res. 4 (3), 247–259.
Ge, X., Fan, Y., Cao, Y., Li, J., Cai, J., Liu, J., Wei, S., 2016. Investigation of organic related pores in unconventional reservoir and its quantitative evaluation. Energy Fuels 30 (6), 4699–4709.
Ginsburg, R.N., 1956. Environmental relationships of grain size and constituent particles in some South Florida carbonate sediments. AAPG (Am. Assoc. Pet. Geol.) Bull. 40, 2384–2427.
Gischler, E., Dietrich, S., Harris, D., Webster, J.M., Ginsburg, R.N., 2013. A comparative study of modern carbonate mud in reefs and carbonate platforms: mostly biogenic, some precipitated. Sediment. Geol. 292, 36–55.
Goral, J., Walton, I., Andrew, M., Deo, M., 2019. Pore system characterization of organic-rich shales using nanoscale-resolution 3D imaging. Fuel 258, 116049.
Hakami, A., İnan, S., 2016. a Basin modeling study of the Jafurah sub-basin, Saudi Arabia: implications for unconventional hydrocarbon potential of the Jurassic Tuwaiq Mountain Formation. Int. J. Coal Geol. 165, 201–222, 2016.
Hakami, A., Al-Mubarak, A., Al-Ramadan, K., Kurison, C., Leyva, I., 2016. Characterization of carbonate mud rocks of the Jurassic Tuwaiq Mountain Formation, Jafurah basin, Saudi Arabia: implications for unconventional reservoir potential evaluation. J. Nat. Gas Sci. Eng. (33), 1149–1168.
Huang, L.K., Wang, M.-J.J., 1995. Pattern Recogn. 28 (1), 41–51.
Harbaugh, J.W., 1967. Carbonate oil reservoir rocks. In: *Developments in sedimentology*, Vol. 9. Elsevier, pp. 349–398.
Huang, L., Ning, Z., Wang, Q., Ye, H., Wang, Z., Sun, Z., Qin, H., 2018. Microstructure and adsorption properties of organic matter in Chinese Cambrian gas shale: experimental characterization, molecular modeling and molecular simulation. Int. J. Coal Geol. 198, 14–28.
Hughes, G.W., 2004. Middle to Upper Jurassic Saudi Arabian carbonate petroleum reservoirs: biostratigraphy, micropalaeontology and palaeoenvironments. GeoArabia 9 (3), 79–114.
Hughes, G.W., 2009. Using Jurassic micropaleontology to determine Saudi Arabian carbonate paleoenvironments. In: Demchuk, D., Gary, A.C. (Eds.), Geologic Problem Solving with Microfossils: A Volume in Honor of Garry D. Jones. SEPM - Society for Sedimentary Geology, Tulsa, Oklahoma, p. 347.
Hughes, G.W., Varol, O., Al-Khalid, M., 2008. Late Oxfordian micropalaeontology, nannopalaeontology a nd palaeoenvironments of Saudi Arabia. GeoArabia 13, 15–46.
Hunt, J.M., 1996. Petroleum Geochemistry and Geology, second ed. W.H. Freeman and Company, New York, p. 743.
Hussain, A., Haughton, P.D., Shannon, P.M., Morris, E.A., Pierce, C.S., Omma, J.E., 2021. Mud-forced turbulence dampening facilitates rapid burial and enhanced preservation of terrestrial organic matter in deep-sea environments. Mar. Petrol. Geol. 130, 105101.
Jarvie, D.M., Claxton, B.L., Henk, F., Breyer, J.T., 2001. Oil and Shale Gas from the Barnett Shale, Fort Worth Basin, vol. 10. AAPG Annual Meeting Program, Texas, p. A100.
Jarvie, D.M., Hill, R.J., Ruble, T.E., Pollastro, R.M., 2007. Unconventional shale-gas systems: the Mississippian Barnett Shale of north-central Texas as one model for thermogenic shale-gas assessment. AAPG (Am. Assoc. Pet. Geol.) Bull. 91, 475–499.
Jiao, K., Yao, S., Liu, C., Gao, Y., Wu, H., Li, M., Tang, Z., 2014. The characterization and quantitative analysis of nanopores in unconventional gas reservoirs utilizing FESEM–FIB and image processing: an example from the lower Silurian Longmaxi Shale, upper Yangtze region, China. Int. J. Coal Geol. 128, 1–11.
Josh, M., Esteban, L., Piane, C.D., Sarout, J., Dewhurst, D.N., Clennell, M.B., 2012. Laboratory characterization of shale properties. J. Petrol. Sci. Eng. 88, 107–124.
Kane, I.A., Pontén, A.S., Vangdal, B., Eggenhuisen, J.T., Hodgson, D.M., Spychala, Y.T., 2017. The stratigraphic record and processes of turbidity current transformation across deep-marine lobes. Sedimentology 64 (5), 1236–1273.
Klaver, J., Hemes, S., Houben, M., Desbois, G., Radi, Z., Urai, J.L., 2015. The connectivity of pore space in mudstones: insights from high-pressure Wood's metal injection, BIBSEM imaging, and mercury intrusion porosimetry. Geofluids. https://doi.org/10.1111/gfl.12128.
Ko, L.T., Loucks, R.G., Ruppel, S.C., Zhang, T., Peng, S., 2017. Origin and characterization of Eagle Ford pore networks in the south Texas Upper Cretaceous shelf. AAPG Bull. 101, 387–418.
Liu, Kouqi, Ostadhassan, Mehdi, Zhou, Jie, Gentzis, Thomas, Rezaee, Reza, 2017. Nanoscale pore structure characterization of the Bakken shale in the USA. Fuel 209, 567–578.
Liu, K., Ostadhassan, M., 2017. Quantification of the microstructures of Bakken shale reservoirs using multi-fractal and lacunarity analysis. J. Nat. Gas Sci. Eng. 39, 62–71.
Loucks, R.G., Reed, R.M., 2014. Scanning-Electron-Microscope Petrographic evidence for distinguishing organic-matter pores associated with depositional organic matter versus migrated organic matter in mudrocks. Gulf Coast Assoc. Geol. Soc. GCAGS J. (3), 51–60.
Loucks, R.G., Reed, R.M., Ruppel, S.C., Jarvie, D.M., 2009. Morphology, genesis, and distribution of nanometer- scale pores in siliceous mudstones of the Mississippian Barnett Shale. J. Sediment. Res. 79, 848–861.
Loucks, R.G., Reed, R.M., Ruppel, S.C., Hammes, U., 2012. Spectrum of pore types and networks in mudrocks and a descriptive classification for matrix-related mudrock pores. AAPG (Am. Assoc. Pet. Geol.) Bull. 96, 1071–1098.
Loucks, R.G., Rowe, H.D., 2014. Upper Cretaceous Niobrara Chalk in Buck Peak Field, Sand Wash Basin, NW Colorado: Depositional Setting, Lithofacies, and Nanopore Network. Extended Abstract, Extended Abstract for paper presented at the Unconventional Resources Technology Conference, Denver, Colorado. https://doi.org/10.15530/urtec-2014-1918913.
Lu, J., Ruppel, S.C., Rowe, H.D., 2015. Organic matter pores and oil generation in the Tuscaloosa marine shale. AAPG Bull. 99, 333–357.
Lucia, F.J., 1983. Petrophysical parameters estimated from visual description of carbonate rocks: a field classification of carbonate pore space. J. Petrol. Technol. 35, 626–637.
Lucia, F.J., 1995. Rock-fabric/petrophysical classification of carbonate pore space for reservoir characterization. AAPG (Am. Assoc. Pet. Geol.) Bull. 79, 1275–1300.
Ma, A.L., Fauchille, L., Dowey, P.J., Pilz, F.F., Courtois, L., Taylor, K.G., Lee, P.D., 2017. Correlative multi-scale imaging of shales: a review and future perspectives. Geol. Soc. Lond., Spec. Publ. 454, SP454, 411.
Ma, Y.Z., Holditch, S., 2015. Unconventional Oil and Gas Resources Handbook: Evaluation and Development. Gulf professional publishing.
Mastalerz, M., Drobniak, A., Stankiewicz, A.B., 2018. Origin, properties, and implications of solid bitumen in source-rock reservoirs: a review. Int. J. Coal Geol. 195, 14–36.
Mayo, S., Josh, M., Nesterets, Y., Esteban, L., Pervukhina, M., Clennell, M.B., et al., 2015. Quantitative micro-porosity characterization using synchrotron micro-CT and xenon K-edge subtraction in sandstones, carbonates, shales and coal. Fuel 154, 167–173.
McClelland, H.L.O., Bruggeman, J., Hermoso, M., Rickaby, R.E.M., 2017. The origin of carbon isotope vital effects in coccolith calcite. Nat. Commun. https://doi.org/10.1038/ncomms14511.
Mehmani, A., Prodanović, M., 2014. The effect of microporosity on transport properties in porous media. Adv. Water Resour. 63, 104–119.
Michaels, J., Budd, D.A., 2014. Pore Systems of the B Chalk Zone in the Niobrara Formation, Denver-Julesburg Basin, Colorado. Extended Abstract for paper presented at the Unconventional Resources Technology Conference, Denver, Colorado. https://doi.org/10.15530/urtec-2014-1922247. August 25-27.
Milliken, K.L., Rudnicki, M., Awwiller, D.N., Zhang, T., 2013. Organic matter-hosted pore system, marcellus formation (Devonian), Pennsylvania, USA. AAPG Bull. 97, 177–200.
Milliken, K.L., Ko, L., Pommer, M., Marsaglia, K.M., 2014. SEM petrography of eastern Mediterranean sapropels: analogue data for assessing organic matter in oil and gas shales. J. Sediment. Res. 84, 961–974.

Moshrif, M.A., 1984. Sequential development of Hanifa formation (upper Jurassic) paleoenvironments and paleogeography, Central Saudi Arabia. J. Petrol. Geol. 7, 451–460.
Murris, R.J., 1980. Middle East stratigraphic evolution and oil habitat. AAPG Bull. 64, 597–618.
Nelson, P.H., 2009. Pore throat sizes in sandstones, tight sandstones, and shales: American Association of Petroleum Geologists. Bulletin 93, 1–13.
O'Brien, N.R., McRobbie, C.A., Slatt, R.M., Baruch- Jurado, E.T., 2016. Unconventional gas–oil shale microfabric features relating to porosity, storage, and migration of hydrocarbons. In: Olson, T. (Ed.), Imaging Unconventional Reservoir Pore Systems: AAPG Memoir 112, pp. 43–64.
Okla, S.M., 1983. Microfacies of Hanifa formation (upper Jurassic) in central Tuwaiq mountains. J. College of Sci. King Saud University 14, 121–143.
Okla, S.M., 1986. Litho- and microfacies of Upper Jurassic carbonate rocks outcropping in Central Saudi Arabia. J. Petrol. Geol. 9, 195–206.
Pirrie, D., Butcher, A.R., Power, M.R., Gottlieb, P., Miller, G.L., 2004. Rapid quantitative mineral and phase analysis using automated scanning electron microscopy (QemSCAN); potential applications in forensic geoscience. Geol. Soc. London, Spec. Public. 232 (1), 123–136.
Pommer, M., Milliken, K.L., 2015. Pore types and pore-size distributions across thermal maturity. Eagle Ford Formation, southern Texas: AAPG (Am. Assoc. Pet. Geol.) Bull. 99, 1713–1744.
Powers, R.W., 1968. Saudi Arabia (Excluding the Arabian Shield). Lexique Stratigraphique International III, Paris.
Powers, R.W., Ramirez, L.F., Redmond, C.D., Elberg, E.L.J., 1966. Geology of the Arabian Peninsula: Sedimentary Geology of Saudi Arabia. U.S. Geological Survey Professional Paper 560–D.
Radwan, A.E., Trippetta, F., Kassem, A.A., Kania, M., 2021. Multi-scale characterization of unconventional tight carbonate reservoir: Insights from October oil filed, Gulf of Suez rift basin, Egypt. J. Petrol. Sci. Eng. 197, 107968 https://doi.org/10.1016/j.petrol.2020.107968.
Radwan, A.E., Wood, D.A., Mahmoud, M., Tariq, Z., 2022. Gas adsorption and reserve estimation for conventional and unconventional gas resources. Chapter 12. In: Wood, D.A., Cai, J. (Eds.), Sustainable geoscience for natural gas sub-surface systems. Elsevier, pp. 345–382. https://doi.org/10.1016/B978-0-323-85465-8.00004-2.
Rahner, M.S., Halisch, M., Fernandes, C.P., Weller, A., dos Santos, V.S.S., 2018. Fractal dimensions of pore spaces in unconventional reservoir rocks using X-ray nano-and micro-computed tomography. J. Nat. Gas Sci. Eng. 55, 298–311.
Reed, R.M., Loucks, R.G., 2007. Imaging nanoscale pores in the mississippian Barnett shale of the northern Fort Worth Basin (abs): American association of petroleum geologists. Annual Convention, Abstracts 16, 115.
Reed, R.M., Loucks, R.G., Ruppel, S.C., 2012. Comment on "Formation of nanoporous pyrobitumen residues during maturation of the Barnett Shale (Fort Worth Basin)" by Bernard et al. (2012). Int. J. Coal Geol. 127, 111–113.
Rine, J.M., Smart, E., Dorsey, W., Hooghan, K., Dixon, M., 2013. Comparison of porosity distribution within selected North American shale units by SEM examination of Argon- ion-milled samples. In: Camp, W.K., Diaz, E., Wawak, B. (Eds.), Electron Microscopy of Shale Hydrocarbon Reservoirs: AAPG Memoir 102, pp. 137–152.
Rouquerol, J., Avnir, D., Fairbridge, C.W., Everett, D.H., Haynes, J.H., Pernicone, N., Sing, J.D.F., Unger, K.K., 1994. Recommendations for the characterization of porous solids. Pure Appl. Chem. 66, 1739–1758.
Ruppel, S.C., Loucks, R.G., 2008. Black mudrocks: Lessons and questions from the mississippian Barnett shale in the southern mid-continent. Sediment. Rec. 6, 4–8.
Sarg, J.F., 1988. Carbonate sequence stratigraphy. In: Wilgus, C.K., Hastings, B.S., Kendall, C.G. St C., Posamentier, H.W., Ross, C.A., Van Wagoner, J.C. (Eds.), Sea-Level Changes: an Integrated Approach: SEPM Special Publication No. 42. SEPM, Tulsa, Oklahoma, pp. 155–181.
Sanaei, A., Ma, Y., Jamili, A., 2019. Nanopore confinement and pore connectivity considerations in modeling unconventional resources. J. Energy Resour. Technol. 141 (1).
Schneider, C.A., Rasband, W.S., Eliceiri, K.W., 2012. NIH Image to ImageJ: 25 years of image analysis. Nat. Methods 9 (7), 671–675. https://doi.org/10.1038/nmeth.2089. PMC 5554542. PMID 22930834.
Schieber, J., 2013. SEM observations on ion-milled samples of Devonian black shales from Indiana and New York: the petrographic context of multiple pore types W. In: Camp, E. Diaz, Wawak, B. (Eds.), Electron Microscopy of Shale Hydrocarbon Reservoirs, vol. 102. AAPG Memoir, pp. 153–171.
Schieber, J., Lazar, R., Bohacs, K., Klimentidis, B., Dumitrescu, M., Ottmann, J., 2016. An SEM study of porosity in the Eagle Ford Shale of Texas— pore types and porosity distribution in a depositional and sequence stratigraphic context. In: Breyer, J.A. (Ed.), The Eagle Ford Shale: A Renaissance in U.S. Oil Production: AAPG Memoir 110, pp. 167–186.
Sharland, P.R., Archer, R., Casey, D.M., Davies, R.B., Hall, S.H., Heward, A.P., Horbury, A.D., Simmons, M.D., 2001. Arabian Plate Sequence Stratigraphy: GeoArabia Special Publication 2. Gulf PetroLink, Bahrain, p. 371.
Slatt, R.M., O'Brien, N.R., 2011. Pore types in the Barnett and Woodford gas shales: contribution to understanding gas storage and migration pathways in fine-grained rocks. AAPG (Am. Assoc. Pet. Geol.) Bull. 95, 2017–2030.
Slatt, R.M., O' Brien, N., Molinares-Blanco, C., Serna-Bernal, A., Torres, E., Philp, P., 2013. Pores, spores, pollen and pellets: small, but significant constituents of resource shales. Unconv. Resour. Technol. Conf. https://doi.org/10.1190/urtec2013-065.
Sohail, G.M., Radwan, A.E., Mahmoud, M., 2022. A review of Pakistani shales for shale gas exploration and comparison to North American shale plays. Energy Rep. 8, 6423–6442. https://doi.org/10.1016/j.egyr.2022.04.074.
Song, L., Carr, T.R., 2020. The pore structural evolution of the Marcellus and Mahantango shales, Appalachian Basin. Mar. Petrol. Geol. 114, 104226.
Syahputra, M.R.N., Eltom, H.A., El-Husseiny, A., Kaminski, M.A., Alqubalee, A.M., 2022. Spatial patterns variations of a burrowed carbonate stratum (ramp carbonates), Upper Jurassic Hanifa Formation, central Saudi Arabia. Sediment. Geol. 435, 106146.
Tang, X., Jiang, Z., Jiang, S., Li, Z., 2016. Heterogeneous nanoporosity of the Silurian Longmaxi Formation shale gas reservoir in the Sichuan Basin using the QEMSCAN, FIB-SEM, and nano-CT methods. Mar. Petrol. Geol. 78, 99–109.
Taylor, K.G., Macquaker, J.H.S., 2000. Early diagenetic pyrite morphology in a mudstonedominated succession: the lower Jurassic cleveland ironstone formation, eastern England. Sediment. Geol. 131, 77–86.
Weijermars, R., Jin, M., Khamidy, N.I., 2021. Workflow for probabilistic resource estimation: Jafurah Basin case study (Saudi Arabia). Energies 14, 8036. https://doi.org/10.3390/en14238036.
Yu, H., Zhu, Y., Jin, X., Liu, H., Wu, H., 2019. Multiscale simulations of shale gas transport in micro/nano-porous shale matrix considering pore structure influence. J. Nat. Gas Sci. Eng. 64, 28–40.
Yang, Y., Liu, X., Zhang, H., Zhai, G., Zhang, J., 2019. A review and research on comprehensive characterization of microscopic shale gas reservoir space. China Geology 3 (4), 1–16. https://doi.org/10.31035/cg2018116.
Yan, S.O.N.G., Zhuo, L.I., Jiang, Z., Qun, L., Dongdong, L., Zhiye, G., 2017. Progress and development trend of unconventional oil and gas geological research. Petrol. Explor. Dev. 44 (4), 675–685.
Zhang, Q., Wu, X.S., Radwan, A.E., et al., 2022. Diagenesis of continental tight sandstone and its control on reservoir quality: A case study of the Quan 3 member of the cretaceous Quantou Formation, Fuxin uplift, Songliao Basin. Mar. Petrol. Geol. 105883. https://doi.org/10.1016/j.marpetgeo.2022.105883.